Available online at www.sciencedirect.com
ScienceDirect
Journal of Power Sources 172 (2007) 460–467
JOURNAL OF POWER SOURCES
www.elsevier.com/locate/jpowsour

Textural and electrochemical characterization of porous carbon nanofibers as electrodes for supercapacitors

Chao-Wei Huang, Yung-Tai Wu, Chi-Chang Hu, Yuan-Yao Li *

Department of Chemical Engineering, National Chung Cheng University, Chia-Yi 621, Taiwan

Received 16 April 2007; received in revised form 28 June 2007; accepted 6 July 2007
Available online 12 July 2007

Abstract

Porous carbon nanofibers (CNFs) enriched with the graphitic structure were synthesized by thermal decomposition from a mixture containing polyethylene glycol and nickel chloride (catalyst). The textural and electrochemical properties of porous CNFs were systematically compared with those of commercially available multi-walled carbon nanotubes (MWCNTs). The high ratio of mesopores and large amount of open edges of porous CNFs with a higher specific surface area, very different from that of MWCNTs, are favorable for the penetration of electrolytes meanwhile the graphene layers of porous CNFs serve as a good electronic conductive medium of electrons. The electrochemical properties of porous CNFs and MWCNTs were characterized for the application of supercapacitors using cyclic voltammetry, galvanostatic charge–discharge method, and electrochemical impedance spectroscopic analyses. The porous CNFs show better capacitive performances ($C_S = 98.4\,F\,g^{-1}$ at $25\,mV\,s^{-1}$ and an onset frequency of behaving as a capacitor at 1.31 kHz) than that of MWCNTs ($C_S = 17.8\,F\,g^{-1}$ and an onset frequency at 1.01 kHz). This work demonstrates the promising capacitive properties of porous CNFs for the application of electrochemical supercapacitors.

Keywords: Mesopore; Carbon nanofibers; Textural and electrochemical properties; Supercapacitors

1. Introduction

Electrochemical supercapacitors have been recognized as an efficient storage device for electric power because of its higher power densities than batteries and higher energy densities than electrolytic capacitors [1,2]. The relatively high energy density of supercapacitors depended on either the low-density materials with high specific surface areas providing the electrical double-layer capacitance (non-Faradic process) [1–7] or the electroactive materials with high Faradaic pseudocapacitance [8–10]. The former devices are usually called electric double-layer capacitors (EDLCs), in which the capacitance comes from the electrolyte-electrode interface. The latter devices are called pseudocapacitors or captteries because the mechanism of energy storage within the electroactive materials is very similar to that of rechargeable batteries [1]. The energy storage system by a non-Faradaic process promises a fast charge/discharge rate, making the EDLCs the best candidate for the demand of high power and long durability.

One-dimensional carbon nanomaterials such as carbon nanotubes (CNTs) [6] and activated carbon nanofiber (ACNFs) [11–15] recently have been studied extensively as an electrode material for EDLCs, because of its unique physico-chemical properties, such as large specific surface area, good electronic conductivity, and chemically stability in different solutions at wide temperature range [16,17]. The performances of EDLCs are dominated by the specific surface area and electronic conductivity of carbon materials. The increase of specific surface of carbon nanomaterials usually uses either physical or chemical activation methods. Physical activation utilizes steam or carbon monoxide as activating agents to create pore texture [11,12,18–20]. Chemical activation with alkali compounds such as KOH or NaOH is a well-known technique to activate carbon materials with porous texture [13–15,21,22]. The pores created by activation are usually in the range of micropores (pore size <2 nm), which are inappropriate for the usage in EDLCs due to the slow rate of electrolyte diffusion. Since the size of hydrated ions is in the range of 6–7.6 Å, the minimum effective pore size should be greater than 15 Å [6]. Several studies revealed that

* Corresponding author. Tel.: +886 5 2720411x33403; fax: +886 5 2721206.
E-mail address: chmyyl@ccu.edu.tw (Y.-Y. Li).

0378-7753/$ – see front matter © 2007 Elsevier B.V. All rights reserved.
doi:10.1016/j.jpowsour.2007.07.009

pore sizes in the range of 30 ± 50 Å are required to maximize the capacitance in the EDLCs [23–25]. In contrast, if the pores are in the range of macropores (>50 nm), the hydrated ions are usually loosely bound to the surface layer and do not particularly contribute to the capacitance [6]. In order to create mesopores in carbon materials, template synthetic process is usually adopted. However, the method is complex and time-consuming since the templates need to be removed. Apart from the effect of pore size, the graphitic structure of the pore wall (edge) is also important to the efficiency of capacitance storage/delivery [26]. It has been claimed that the edge of the hexagon provides a more effective surface than the basal plane [27–30]. As a result, a simple method to fabricate of one-dimensional carbon nanomaterials with mesoporous and graphitic structure are required for the above purposes so that the materials will be a promising candidate for the electrode material in EDLCs. Based on the above considerations, porous carbon nanofibers (CNFs) is one of the candidates better than CNTs for using as an electrode material of EDLCs because of its unique structure, which exhibited graphitic structure, mesopores and open edges (easily to graft oxygen functional groups). Therefore, porous CNFs possess a good electronic conductivity and suitable pore size for electrolyte transport, which is considered as a good medium for the applications of EDLCs.

In this work, we synthesized the porous CNFs from thermal decomposition of poly(ethylene glycol) (PEG) containing catalyst under desired temperature [31]. The nitrogen adsorption isotherm was used to examine the mean pore size and pore size distribution. The synthesized materials and commercial multi-walled carbon nanotubes (MWCNTs) were characterized by high-resolution transmission electron microscopy (HR-TEM), field-emission scanning electron microscopy (FE-SEM), thermogravimetric analysis (TGA), and Raman spectrumeter. The oxygen-containing functional groups on porous CNFs and MWCNTs were characterized by X-ray photoelectron spectroscopy (XPS). The electrochemical behavior of porous CNFs was investigated and compared with that of commercial MWCNTs using cyclic voltammetry (CV), galvanostatic charge-discharge, and electrochemical impedance spectrum (EIS).

2. Experimental

2.1. Preparation of porous CNFs

Porous CNFs were prepared by thermal decomposition from a mixture of PEG and nickel chloride ($NiCl_2$) at 600 °C under nitrogen atmosphere. Details of the preparation process of porous CNFs were described in our previous work [31]. MWCNTs (trade code: CN3003, purity 95%, diameter: 20–40 nm, Seedchem Company PTY.LTD) used here were commercial products prepared by a conventional CVD methods. Two carbon nanomaterials were heated at 440 and 450 °C in air for 30 min in order to remove amorphous carbon and to expose the edge planes. The morphology of carbon nanomaterials was examined by FE-SEM (Hitachi S-4800) while HR-TEM (Philips TECNAI 20) was employed to observe the crystal structure and graphene layers arrangement. The Raman spectra were measured at room temperature using a 3D Nanometer Scale Raman PL Microspectrometer (Tokyo Instruments, Inc., a 632.8 nm He–Ne laser). TGA (Perkin–Elmer, Diamond TG/DTA) was conducted to investigate the oxidative stability of two carbon nanomaterials. Nitrogen adsorption–desorption isotherms were performed by an ASAP 2020 system at 77 K. The samples were degassed under vacuum at 200 °C for 4 h prior to the measurements. XPS measurements were performed with an ESCA PHI 1600 (Perkin–Elmer) spectrometer with Mg Kα radiation ($h\nu$ = 1253.6 eV).

2.2. Electrochemical measurements

Porous CNFs and commercial MWCNTs were served as the basic electrode constituents for the electrochemical investigations for supercapacitor. These carbon derivatives were bound onto 10 mm × l0 mm × 3 mm graphite substrates. Before coating, the substrates were abraded with ultrafine SiC paper, degreased with acetone and water, etched in a 0.1 M HCl solution at room temperature (ca. 26 °C) for 10 min, and finally degreased with water in an ultrasonic bath. The exposed geometric area of these pretreated graphite supports is equal to 1 cm^2 while the other surface areas were insulated with polytetrafluorene ethylene coatings. Electrodes were prepared through the drop coating procedure. Carbon materials were ultrasonically dispersed in a 95 wt.% ethanol solution with the concentration equal to 1 mg cm^{-3}. The well-dispersed solution was dropped onto the pre-treated graphite substrate and dried at 85 °C. The total loading on each electrode was kept approximately constant (ca. 1 mg cm^{-2}) through repeating the above procedure to avoid any unexpected influences. These electrodes were dried in a vacuum oven at 85 °C overnight. The weight of each one-dimensional carbon nanomaterials was measured through a microbalance with an accuracy of 10 μg (Sartorius BP 21 1D, Germany).

Electrochemical measurements were performed by means of an electrochemical analyzer system, CHI 633A (CH Instruments, USA). The EIS analyzer system, IM6 (Zahner) with the Thales software, was employed to measure and analyze the ac impedance spectra. The potential aptitude of ac is equal to 10 mV and its frequency range is from 100 mHz to 10 kHz. All experiments were carried out in a three-compartment cell. An Ag/AgCl electrode (Argenthal, 3 M KCl, 0.207 V versus SHE at 25 °C) was used as the reference and a piece of platinum gauze with an exposed area equal to 4 cm^2 was employed as the counter electrode. A Luggin capillary, whose tip was set at a distance of 1–2 mm from the surface of the working electrode, was used to minimize errors due to iR drop in the electrolyte. The potentiodynamic measurements were performed by means of CV between 0 and 1 V at various scan rates.

All solutions used in this work were prepared with 18 M cm water produced by a reagent water system (MILLI-Q SP, Japan), and all reagents not otherwise specified in this work were Merck, GR. In addition, the electrolytes used to study the capacitive behavior of carbon nanomaterilas were degassed with purified nitrogen gas before measurements, and nitrogen was passed over

the solutions during the measurements. The solution temperature was maintained at 25 °C by means of a water thermostat (HAAKE DC3 and K20).

3. Results and discussion

3.1. Characterization of one dimensional carbon nanomaterials

Fig. 1a and b show the SEM images of porous CNFs and commercial MWCNTs, respectively. Porous CNFs and MWCNTs were 40–60 nm and 20–40 nm in diameters, respectively. AHR-SEM image in Fig. 1c reveals that porous CNFs have rough surface and porous structure, which were different from the MWCNTs. Fig. 2a and b show the HR-TEM images of porous CNFs and commercial MWCNTs, respectively. It can be easily observed in Fig. 2a that the porous CNFs have disorder graphitic structure, graphitic pore walls, and open edges. The pores of porous CNFs have no regular shape and the pore size were about 4–6 nm, which were suitable for the penetration of electrolytes for the application of EDLCs. It also shows obviously in Fig. 2b that the graphene layer of MWCNTs were parallel to the fiber axis and none pores were on the surface.

Fig. 3a and b show the C1s XPS spectra of porous CNFs and MWCNTs, respectively. In order to obtain the quantitative information of oxygen-containing functional groups on porous CNFs and MWCNTs, the software package XPS Peak 4.1 was used to fit the high resolution C1s peak. The C1s spectrum can be decomposed into six peaks centered at 284.5 ± 0.2, 285.1 ± 0.2, 286.2 ± 0.2, 287.5 ± 0.2, 288.9 ± 0.2, and 291 ± 0.2 eV [32–35]. The main peak (peak 1) at 284.5 ± 0.2 eV was assigned to sp^2-hybryidized graphite-like carbon atoms and in carbon atoms bound to hydrogen atoms. Peak 2 at 285.1 ± 0.2 eV can be assigned to sp^3-hybridized carbon atoms as in diamond-like carbon. The peaks 3–5 centered at 286.2 ± 0.2, 287.5 ± 0.2, and 288.9 ± 0.2 eV correspond to hydroxyl, carbonyl (or ether), and carboxyl (or ester), respectively. Peak 6 at 291.0 eV is expected to be the shake up feature of typical aromatic structures [35]. The relative area of these sub-peaks can be used to calculate the relative content of oxygen-containing functional group of porous CNFs and MWCNTs. Table 1 shows the relative content for each peak of the C1s spectra. The relative contents of three oxygen-containing functional groups (peaks 3–5) on porous CNFs are all higher than that on MWCNTs. Due to the fact that the porous CNFs have large amounts of open edges and mesopores, they have more effective surface area than the basal plane of the MWCNTs. This property should be easier to graft functional groups during

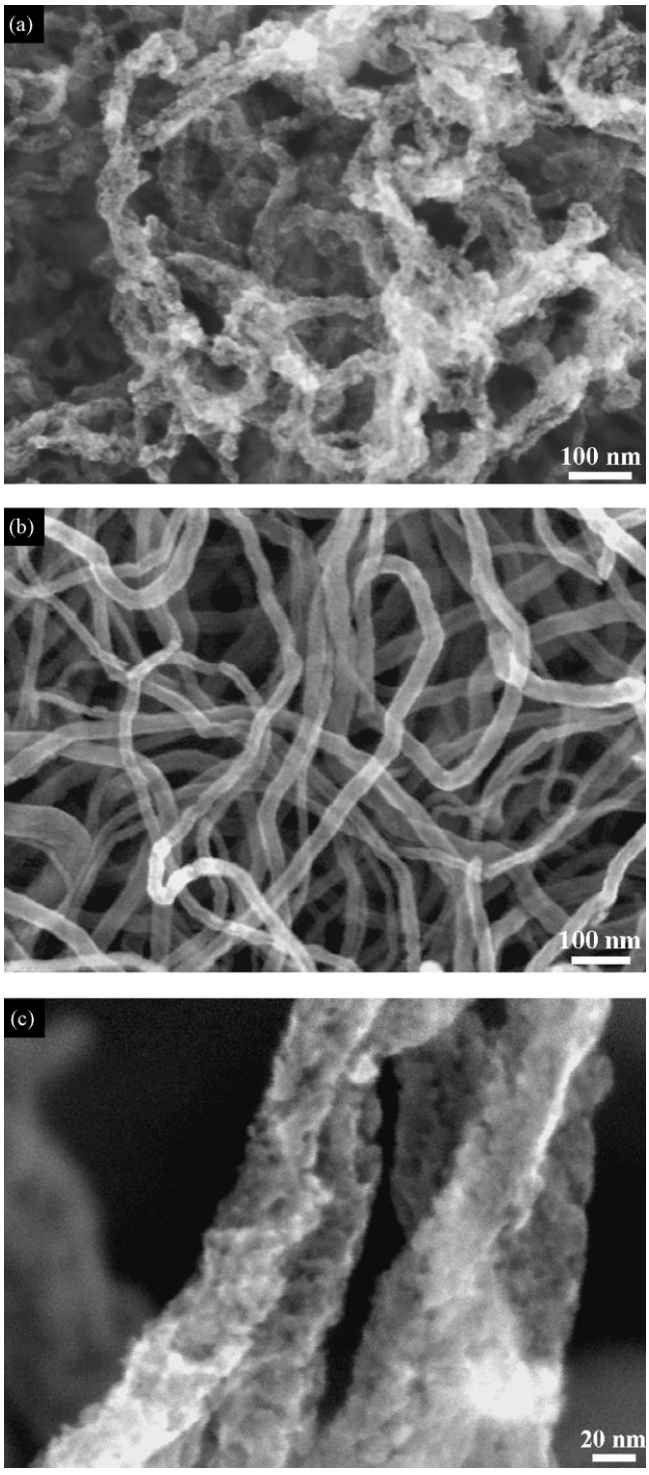

Fig. 1. SEM images of (a) porous CNFs and (b) MWCNTs; (c) HR-SEM image of porous CNFs.

Table 1
Relative content of functional groups in C1s from XPS spectra

Carbon materials	Surface functional group					
	Peak 1 (%)	Peak 2 (%)	Peak 3 (%)	Peak 4 (%)	Peak 5 (%)	Peak 6 (%)
Porous CNFs	60.5	13.8	12.1	6.7	4.1	2.8
MWCNTs	69.6	13.2	7.5	4.0	1.9	3.8

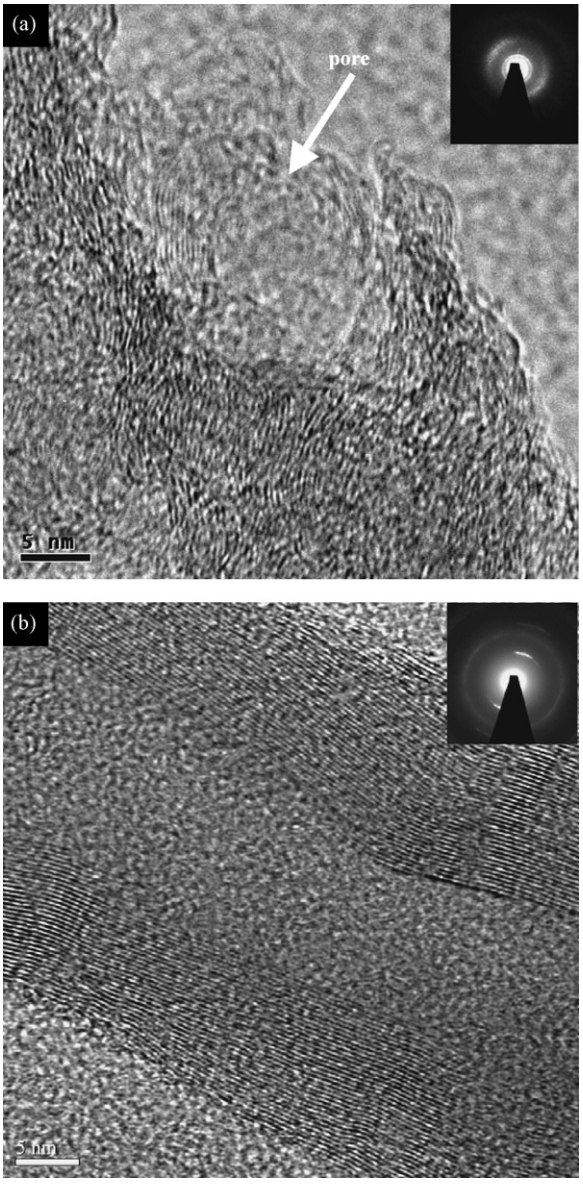

Fig. 2. HR-TEM images of (a) porous CNFs and (b) MWCNTs.

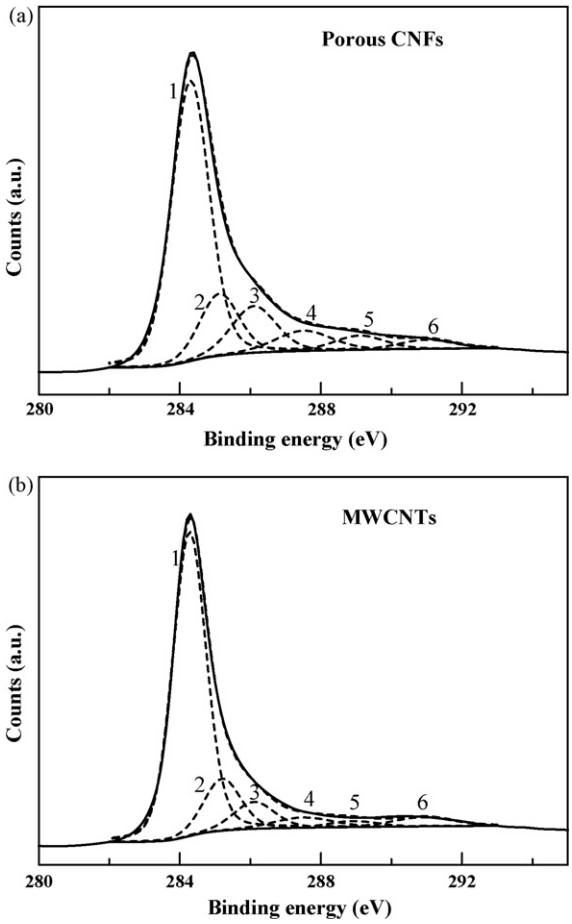

Fig. 3. XPS C1s spectra of (a) porous CNFs and (b) MWCNTs.

the synthesis and purification processes. Therefore, the higher content of oxygen-containing functional groups and the unique textural characteristics of porous CNFs are expected to promote the contribution of pseudo-capacitance and electric double layer capacitance (see below).

Fig. 4 shows the Raman spectra of carbon nanomaterials. Two characteristic peaks that lie at about 1330 and 1590 cm^{-1} correspond to D-band and G-band, respectively. The D-band represents defects, curved graphite sheets, dislocations, and lattice distortions in carbon structures [36]. The G-band is explained as the stretching vibration mode of graphite crystals [37]. The relatively peak intensity of G band to D band of porous CNFs and MWCNTs are about 0.93 and 0.79, respectively. These results suggest that two materials have approximately the same graphitization and electronic conductivity, which can be served as a good electronic conductor. Fig. 5 shows the TGA results of two carbon nanomaterials. Thermal oxidation of porous CNFs and MWCNTs occurs dramatically at the temperature about 500 and 600 °C, respectively, indicating that the edge plane opening of porous CNFs is less stable than the basal plane of MWCNTs. This result further supports the fact that porous CNFs are enriched with the open edges.

The adsorption/desorption isotherms of nitrogen at 77 K on the carbon nanometerials were measured to gain an understanding on the surface area by the BET method [38], pore volume by the single point calculation at a relative pressure

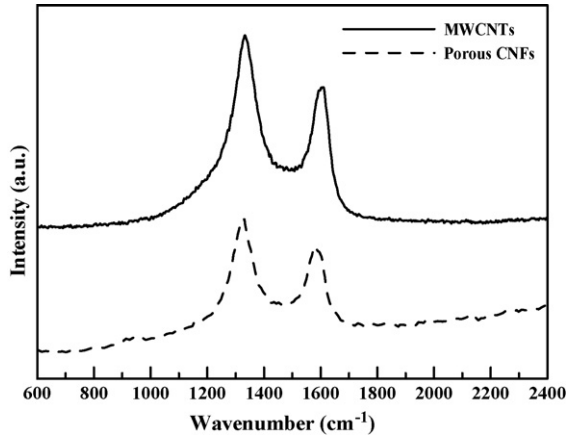

Fig. 4. Raman spectra of porous CNFs and MWCNTs.

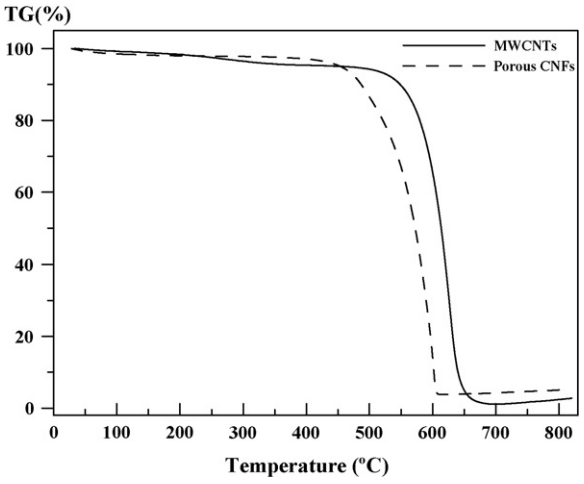

Fig. 5. TGA curves of porous CNFs and MWCNTs.

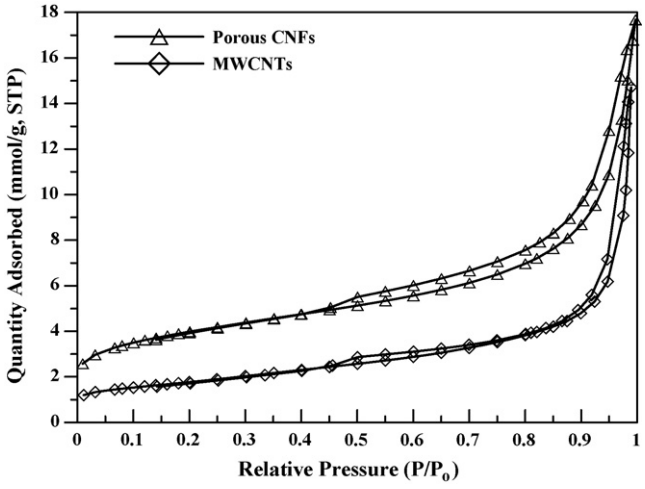

Fig. 6. Nitrogen adsorption/desorption isotherms of porous CNFs and MWCNTs.

of about 0.98, and the mean pore size. Fig. 6 shows nitrogen adsorption/desorption isotherms of porous CNFs and MWCNTs. Both the adsorption/desorption isotherms of porous CNFs and MWCNTs represented the type-II adsorption/desorption characteristics. The pore characteristics of both carbon nanomaterials are shown in Table 2. The results show that porous CNFs have a larger specific surface area in comparison with that of MWCNTs, mainly contributed by the mesoporous structure.

From all the above analyses, the microstructural characteristics of porous CNFs are beneficial to be used as an electrode material in the supercapacitor application because the graphitic structure of the pore wall (edge) [26] and the high specific surface

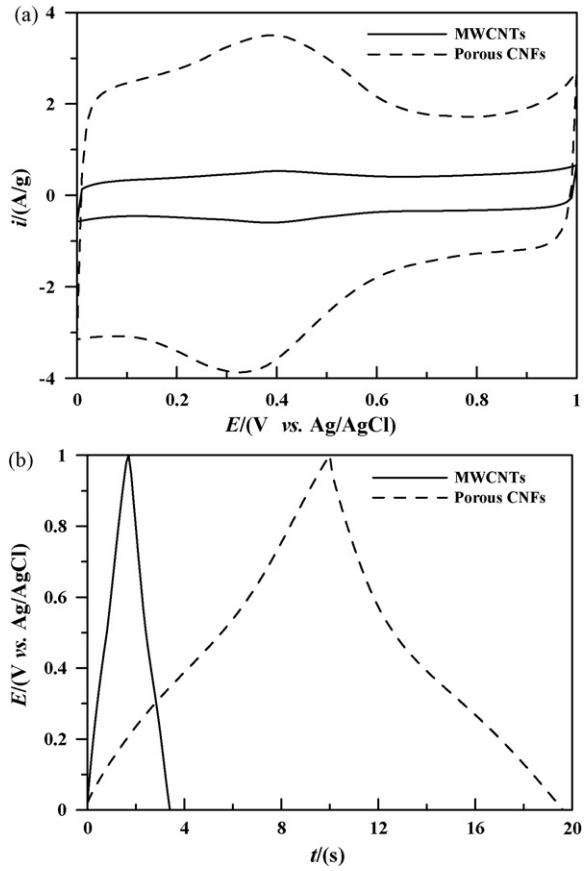

Fig. 7. (a) Cyclic voltammograms of MWCNTs and porous CNFs measured in 1 M H_2SO_4 at 25 mV s^{-1} under 25 °C. (b) Chronopotentiaograms of MWCNTs and porous CNFs measured in 1 M H_2SO_4 at a current density of 10 A g^{-1}.

area of mesopore are positive to the utilization of capacitance during the charging/discharging process [23–25], and the higher content of oxygen-containing functional groups will enhance the contribution of pseudo-capacitance.

3.2. Electrochemical characterization

The capacitive behavior of MWCNTs and porous CNFs, examined by CV (Fig. 7a) at 25 mV s^{-1} and choronopotentiaometry (CP, Fig. 7b) at 10 A g^{-1} in 1 M H_2SO_4, shows the typical *i–E* responses of carbon materials. For both curves in Fig. 7a, the background current density negative to ca. 0.6 V on both positive and negative sweeps with a broad pair of redox peaks around 0.4–0.5 V is much higher than that obtained in the relatively positive potential region. This phenomenon has been attributed to a combination of electrical double-layer charge/discharge and the redox transitions of interfacial oxygen-containing functional

Table 2
Physical characteristics of porous CNFs and MWCNTs

Carbon type	BET surface area (m^2 g^{-1})	Average pore diameter (Å)	Pore volume fraction (%)		Total pore volume (cm^3 g^{-1})
			Micropore	Mesopore	
Porous CNFs	302	62	7	93	0.46
MWCNTs	140	89	0	100	0.31

groups resulting from the synthesis and/or purification processes [16,39,40]. Since the current density of porous CNFs is much larger than that of MWCNTs, the electric energy (and specific capacitance) stored in porous CNFs is much larger than that of MWCNTs. The much higher current density of the former carbon material is attributable to its higher specific surface area and higher content of surface functional groups (see below). The above statement is further supported by the potential-dependent choronopoteniogram of porous CNFs shown in Fig. 7b. For an ideal polarized electrode, the double-layer capacitance is only weakly dependent upon the applied potentials (i.e., $dE/dt \approx$ a constant value). However, the CP responses of porous CNFs do not obey this phenomenon, revealing the significant contribution of redox reactions from surface functional groups although the charge curve is completely symmetric to its discharge counterpart, indicating the excellent reversibility.

From Fig. 7, the specific capacitance of two carbon nanomaterials can be easily estimated according to Eqs. (1) and (2) for CV and CP, respectively:

$$C_s = \frac{q^*}{2w\Delta V} \quad (1)$$

$$C_s = \frac{C}{w} = \frac{i}{|dE/dt|\, w} \approx \frac{i}{(\Delta E/\Delta t)w} \quad (2)$$

where C_s, C, w, i, q^*, ΔV, and $(\Delta E/\Delta t)$ represents the specific capacitance, total capacitance, weight of carbon materials, current density of charge or discharge, integrated charges of CVs, potential window of CV, and mean slope of the charge or discharge curves in the investigated potential range. From CVs shown in Fig. 7a, the specific capacitance of MWCNTs and porous CNFs (measured at 25 mV s^{-1}) is equal to 17.8 and 98.4 F g^{-1}, respectively, which are very close to the values estimated from CPs (measured at 10 A g^{-1}); 17 and 98 F g^{-1}, respectively.

In general, the capacitance contributed by the electrical double layers should be directly proportional to the specific surface area (denoted as S_A) of electrode materials [41–43]. From Table 1, it is clear that S_A of porous CNFs is about two times of that of MWCNTs but its Cs is almost six times of that of MWCNTs. This novel phenomenon may be attributed to a combined effect of the pore structure/distribution and the surface functional group content between these two kinds of carbon nanomaterials. From the SEM images in Fig. 1, the surface of porous CNFs is much rougher than that of MWCNTs, which is enriched with nano-apertures also clearly observed in the TEM photographs in Fig. 2a. In addition, the HR-TEM image and BET analysis reveal that the surface of porous CNFs is irregular and the pore size is mainly distributed from about 4 to 6 nm, which are favorable for the diffusion of hydrated ions during the charge/discharge of the electric double layers [6,23–25]. Furthermore, the higher S_A of porous CNFs should provide more loci for the formation of surface functional groups enhancing the contribution of pseudocapacitance. Therefore, porous CNFs show the unique merit of combining pseudocapacitance and electric double layer capacitance, resulting in their much higher specific capacitance in comparison with MWCNTs.

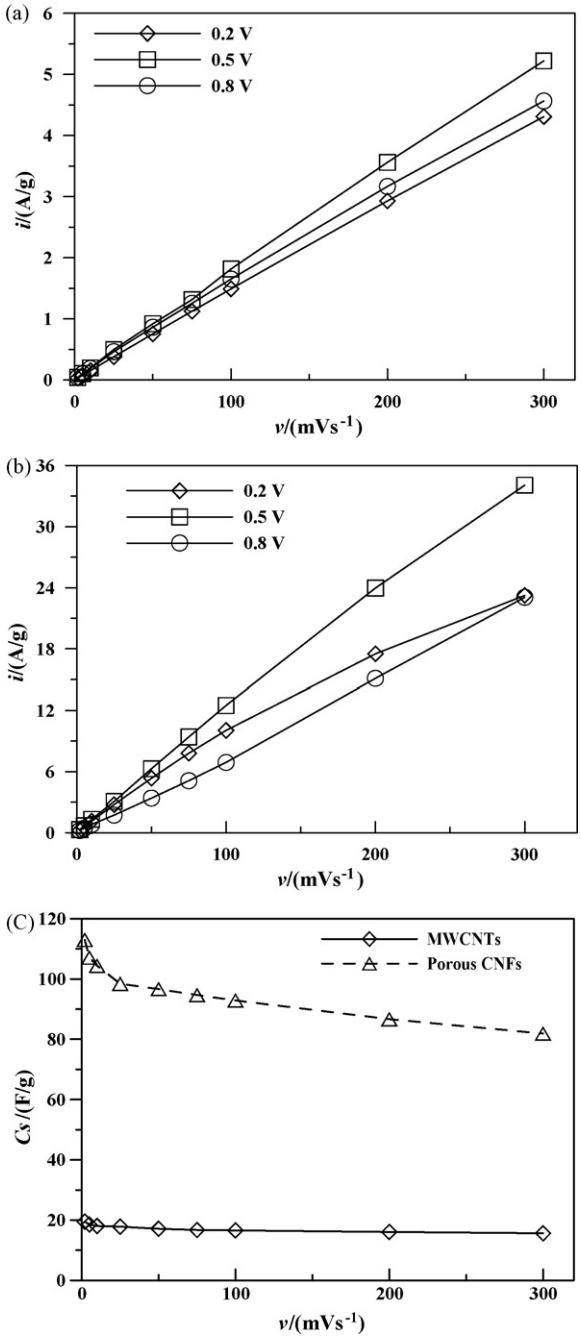

Fig. 8. Dependence of voltammetric currents on the scan rate of CV for (a) MWCNTs and (b) porous CNFs measured in 1 M H_2SO_4; (c) dependence of specific capacitance loss on scan rate of CV from 2 to 300 mV s^{-1}.

One of the main purposes of employing porous CNFs is to improve the power property of carbon-based materials for the supercapacitor application. This effect can be clearly demonstrated from the dependence of capacitive current densities on the scan rate of CV (see Fig. 8a and b). The quasi-linear dependence of the current density on the scan rate varying from 2 to 300 mV s^{-1} does indicate the highly reversible charge/discharge responses of both MWCNTs and porous CNFs in 1M H_2SO_4. This result is reasonably attributed to the mesoporous nature of both carbon materials, resulting in the high ionic conductivity

within the electrode materials. In addition, the superficial redox transitions of electroactive groups with highly electrochemical reversibility have been proposed as follow [1,16]:

$$O{=}Ph{=}O + 2H^+ + 2e \leftrightarrow HO{-}Ph{-}OH \quad (3)$$

$$R{=}O + H^+ + e \leftrightarrow R{-}OH \quad (4)$$

where Ph and R indicate the phenyl and aliphatic groups, respectively. Hence, both materials show the high-power property, satisfying one of the basic requirements for the electrode materials of supercapacitors.

Fig. 8c shows the dependence of specific capacitance of MWCNTs and porous CNFs on the scan rate of CV obtained in 1 M H_2SO_4. The specific capacitance of porous CNFs is gradually decreased from ca. 113 to 82 F g^{-1} when the scan rate of CV is increased from 2 to 300 mV s^{-1}, indicating a 28% loss in C_S. A similar but less obvious phenomenon is found for MWCNTs, revealing a smaller loss in the specific capacitance (ca. 20%). The above minor dependence of the electrochemically accessible area on the scan rate of CV reflects the feasibility in building the electric double layers within mesopores and the high redox reversibility of surface functional groups. This important merit of carbons mainly consisted of mesopores (i.e., porous CNFs and MWCNTs) is very different from the charge/discharge behavior of activated carbons enriched with micropores [44]. Note that the specific capacitance of porous CNFs is always much larger than that of MWCNTs in the whole range of scan rates meanwhile the quasi-linear dependence of i on the scan rate of CV is visible for both carbon nanomaterials. These results indicates the much higher energy and power densities of porous CNFs is comparison with that of MWCNTs even when the scan rate is up to 300 mV s^{-1}.

The EIS analysis, representing as Nyquist plots (see Fig. 9), is used to demonstrate the unique capacitive characteristics of porous CNFs. Since MWCNTs generally show excellent EIS responses in aqueous media, the result measured from this material is used for a comparison purpose. Note that the equivalent series resistance (ESR) of the porous CNFs electrode, estimated from the diameter of the impedance arc in the high-frequency region, is close to that of MWCNTs. This result indicates that the ESR of porous CNFs is as low as that of MWCNTs, which are an excellent electronic conductor [45]. This phenomenon is reasonably due to the enriched graphitic structure of the pore walls for both materials. In the medium frequency region, the "onset" frequency for the MWCNTs electrode behaving as a capacitor is equal to ca. 1.04 kHz. Since the onset frequency is defined as the frequency where the lowest image impedance occurs or the frequency where the impedance starts to be dominated by the image (capacitor) part in the medium frequency region, MWCNTs are considered to behave as a capacitor behind this frequency. Moreover, the higher the onset frequency of an electrode material is, the higher power density of this material can be achieved. Accordingly, the higher onset frequency (1.31 kHz Hz) of porous CNFs reveals its higher power property than that of MWCNTs, which is consistent with the results obtained from CVs. Also note that the impedance of the porous CNFs electrode (i.e., dashed-line curve) in the image part measured at any specified frequency is smaller than that of the MWCNTs (i.e., solid-line curve). This result accounts for the higher specific capacitance of the porous CNFs electrode, which is consistent with the CV and CP results. All the above results reveal that porous CNFs with low ESR, high power characteristics, and excellent maintenance of specific capacitance under the high power operation is a promising electrode material for the application of supercapacitors.

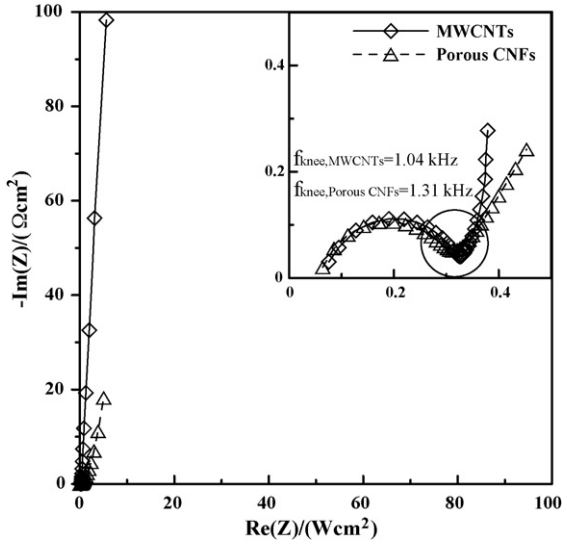

Fig. 9. Nyquist plots for (a) MWCNTs (solid-line) and (b) porous CNFs (dashed-line) electrodes measured at 0.5 V in 1 M H_2SO_4. Inset: Data in the high-frequency region.

4. Conclusions

In this study, porous CNFs enriched with the graphitic structure, mesopores (4–6 nm), and open edges were prepared from thermal decomposition of a mixture containing PEG and $NiCl_2$. The enriched open edges of porous CNFs are easier to graft the oxygen functional groups than the basal-planes of MWCNTs. Porous CNFs are of good electronic conductivity, higher specific surface, suitable pore size, and higher content of surface oxygen functional groups. These unique properties of porous CNFs are favorable for the diffusion of hydrated ions during the charge/discharge within the electric double layers and provide more effective surface area than the basal plane of MWCNTs. The specific capacitance of porous CNFs measured at 25 mV s^{-1} in 1 M H_2SO_4 is 98.4 F g^{-1} which is six times of that of commercial MWCNTs. The charge/discharge responses of porous CNFs are as ideal as that of MWCNTs although the surface of the former materials is enriched with oxygen-containing functional groups providing significant pseudo-capacitance. From the EIS study, the electronic conductivity of porous CNFs is very similar to that of MWCNTs meanwhile the onset frequency (1.31 kHz Hz) of porous CNFs behaving as a capacitor is higher than that of MWCNTs (1.01 kHz Hz). The low ESR, high power characteristics, and excellent maintenance of specific capacitance under the high power operation elucidate that porous CNFs are a beneficial electrode material for the supercapacitor application.

Acknowledgement

The financial support of this work by the National Science Council of ROC is gratefully acknowledged.

References

[1] B.E. Conway, Electrochemical Supercapacitors, Kluwer-Plenum Publishing Co., New York, 1999.
[2] A. Burke, J. Power Sources 91 (2000) 37.
[3] Y.R. Nian, H. Teng, J. Electrochem. Soc. 149 (2002) A1008.
[4] Y. Kibi, T. Saito, M. Kurata, J. Tabuchi, A. Ochi, J. Power Sources 60 (1996) 219.
[5] D. Qu, H. Shi, J. Power Sources 74 (1998) 99.
[6] K.H. An, W.S. Kim, Y.S. Park, J.M. Moon, D.J. Bae, S.C. Lim, Y.S. Lee, Y.H. Lee, Adv. Funct. Mater. 11 (2001) 387.
[7] C.T. Hsieh, Y.T. Lin, Micropor. Mesopor. Mat. 93 (2006) 232.
[8] C.C. Hu, Y.H. Huang, J. Electrochem. Soc. 146 (1999) 2465.
[9] C.C. Hu, K.H. Chang, Electrochim. Acta 45 (2000) 2685.
[10] C.C. Hu, T.W. Tsou, Electrochem. Comm. 4 (2002) 105.
[11] C. Kim, J. Power Sources 142 (2005) 382.
[12] C. Kim, K.S. Yang, Appl. Phys. Lett. 83 (2003) 1216.
[13] C. Merino, P. Soto, E. Vilaplana-Ortego, J.M. Gomez de Salazar, F. Pico, J.M. Rojo, Carbon 43 (2005) 551.
[14] S.U. Kim, K.H. Lee, Chem. Phys. Lett. 400 (2004) 253.
[15] Y.J. Kim, Y. Horie, Y. Matsuzawa, S. Ozaki, M. Endo, M.S. Dresselhaus, Carbon 42 (2004) 2423.
[16] K. Kinoshita, Carbon: Electrochemical and Physicochemical Properties, Wiley, New York, 1988.
[17] E. Frackowiak, F. Béguin, Carbon 39 (2001) 937.
[18] S. Lim, S.H. Hong, W. Qiao, D. Duayne Whitehurst, S.H. Yoon, I. Mochida, B. An, K. Yokogawa, Carbon 45 (2007) 173.
[19] P. Li, T.J. Zhao, J.H. Zhou, Z.J. Sui, Y.C. Dai, W.K. Yuan, Carbon 43 (2005) 2701.
[20] M. Suzuki, Carbon 32 (1994) 577.
[21] S.H. Yoon, S. Lim, Y. Song, Y. Ota, W. Qiao, A. Tanaka, I. Mochida, Carbon 42 (2004) 1723.
[22] D. Luxembourg, X. Py, A. Didion, R. Gadiou, C. Vix-Guterl, G. Flamant, Micropor. Mesopor. Mat. 98 (2007) 123.
[23] S.T. Mayer, R.W. Pekala, J.L. Kaschmitter, J. Electrochem. Soc. 140 (1993) 446.
[24] I. Tanahashi, A. Yoshida, A. Nishino, J. Electrochem. Soc. 137 (1990) 3052.
[25] B. Kastening, S. Sprinzig, J. Electroanal. Chem. 214 (1986) 295.
[26] S. Mitani, S.I. Lee, K. Saito, Y. Korai, I. Mochida, Electrochim. Acta 51 (2006) 5487.
[27] H.H. Bauer, M.S. Spritzer, P.J. Elving, J. Electroanal. Chem. 17 (1968) 299.
[28] J.P. Randin, E. Yeager, J. Electrochem. Soc. 118 (1971) 711.
[29] J.P. Randin, E. Yeager, J. Electroanal. Chem. 36 (1972) 257.
[30] J.P. Randin, E. Yeager, J. Electroanal. Chem. 58 (1975) 313.
[31] C.W. Huang, W.H. Lin, Y.Y. Li, Unpublished results.
[32] J.H. Zhou, Z.J. Sui, J. Zhu, P. Li, D. Chen, Y.C. Dai, W.K. Yuan, Carbon 45 (2007) 785.
[33] H. Ago, T. Kugler, F. Cacialli, W.R. Salaneck, M.S.P. Shaffer, R.H. Friend, A.H. Windle, J. Phys. Chem. B 103 (1999) 8116.
[34] C. Pirlot, I. Willems, A. Fonseca, J.B. Nagy, J. Delhalle, Adv. Eng. Mater. 4 (2002) 109.
[35] G. Beamson, D. Briggs, High Resolution XPS of Organic Polymers. The Scienta ESCA A300 Database, Wiley, Chichester, 1992.
[36] F. Tuinstra, J.L. Koenig, J. Chem. Phys. 53 (1970) 1126.
[37] A. Kasuya, Y. Sasaki, Y. Saito, Y. Kohji, Y. Nishina, Phys. Rev. Lett. 78 (1997) 4434.
[38] S. Brunauer, P.H. Emmett, E. Teller, J. Am. Chem. Soc. 60 (1938) 309.
[39] M. Muller, B. Kastening, J. Electroanal. Chem. 374 (1994) 149.
[40] A. Rudge, J. Davey, I. Raistrick, S. Gottesfeld, J.P. Ferrais, J. Power Sources 47 (1994) 89.
[41] O. Barbieri, M. Hahn, A. Herzog, R. Kötz, Carbon 43 (2005) 1303.
[42] T.C. Weng, H.S. Teng, J. Electrochem. Soc. 148 (2001) 368.
[43] D. Lozano-Castello, D. Cazorla-Amoros, A. Linares-Solano, S. Shiraishi, H. Kurihara, A. Oya, Carbon 41 (2003) 1765.
[44] F.C. Wu, R.L. Tseng, C.C. Hu, C.C. Wang, J. Power Sources 144 (2005) 302.
[45] P.J.F. Harris, Carbon Nanotubes and Related Structures: New Materials for the 21st Century, Cambridge University Press, Cambridge, UK, 1999, pp. 115–134.